GA–A27389

3D VACUUM MAGNETIC FIELD MODELING OF THE ITER ELM CONTROL COILS DURING STANDARD OPERATING SCENARIOS

by
T.E. EVANS, D.M. ORLOV, A. WINGEN, W. WU, A. LOARTE, T.A. CASPER,
O. SCHMITZ, G. SAIBENE, and M.J. SCHAFFER

AUGUST 2012

GENERAL ATOMICS

DISCLAIMER

GA–A27389

3D VACUUM MAGNETIC FIELD MODELING OF THE ITER ELM CONTROL COILS DURING STANDARD OPERATING SCENARIOS

by
T.E. EVANS, D.M. ORLOV,* A. WINGEN,† W. WU, A. LOARTE,‡ T.A. CASPER,‡
O. SCHMITZ,# G. SAIBENE,¶ and M.J. SCHAFFER

This is a preprint of a paper to be presented at the Twenty-fourth IAEA Fusion Energy Conf., October 8-13, 2012 in San Diego, California.

*University of California San Diego, La Jolla, California, USA.
†Oak Ridge National Laboratory, Oak Ridge, Tennessee, USA.
‡ITER Organization, 13115 St Paul lez Durance, France.
#Forschungszentrum Jülich, IEF-4 Euratom Association, Jülich, Germany.
¶Fusion for Energy Joint Undertaking, Barcelona, Spain.

Work supported in part by
UT BATTELLE, LLC under 4000095588 and
the U.S. Department of Energy under
DE-AC05-00OR22725, DE-FG02-05ER54809, DE-FG02-07ER54917,
and the ITER Task Agreement C19TD42FU

GENERAL ATOMICS PROJECT 39373
AUGUST 2012

3D Vacuum Magnetic Field Modeling of the ITER ELM Control Coils During Standard Operating Scenarios

T.E. Evans 1), D.M. Orlov 2), A. Wingen 3), W. Wu 1), A. Loarte 4), T.A. Casper 4), O. Schmitz 5), G. Saibene 6) and M.J. Schaffer 1)

1) General Atomics, PO Box 85608, San Diego, California 92186-5608, USA
2) University of California San Diego, La Jolla, California 92093-0417, USA
3) Oak Ridge National Laboratory, PO Box 2008, Oak Ridge, Tennessee 37831-8072, USA
4) ITER Organization, Route de Vinon sur Verdon, 13115 St Paul lez Durance, France
5) Forschungszentrum Jülich, IEF-4 Euratom Association, Jülich, Germany
6) Fusion for Energy Joint Undertaking, Barcelona, Spain

e-mail contact of main author: evans@fusion.gat.com

Abstract. In-vessel, non-axisymmetric, control coils have proven to be an important option for mitigating and suppressing edge-locaized modes (ELMs) in high performance operating regimes on a growing number of tokamaks. Recently, an in-vessel non-axisymmertic ELM control coil has been included in the ITER baseline design. In preparing for the initial operation of this coil, a comprehensive study has been carried out to characterize the linear superposition of the 3D vacuum magnetic field, produced by ELM coils, on a series of equilibria representing 9 standard ITER operating scenarios. Here, the spatial phase angle of toroidally distributed currents, specified with cosine waveform, in the upper and lower rows of the ITER ELM coils is varied in 2º steps while holding the phase angle of the currents in the equatorial plane coils constant. The peak current in each of the 3 toroidal rows of coils is scanned between 5 kAt and 90 kAt and the width of the edge region, covered by overlapping magnetic islands, is calculated. This width is compared to a correlation criterion found in DIII-D for ELM suppression for each ELM coil current level and phase angle setting. A minimum coil current satisfying the DIII-D criterion, along with an associated set of phase angles, is identified for each ITER operating scenario. It is found that the minimum current required to satisfy the DIII-D correlation criterion varies from 20 kAt to 50 kAt depending on the operating scenario and the toridal mode number (n) of the cosine waveform used. It is also found that the DIII-D correlation criterion for ELM suppression can be satisfied, in the most demanding ITER scenario, with n=3 perturbation fields and with up to 8 malfunctioning coils out of the full set of 27. In addition, it is found that operating the ELM coils with the 8 malfunctioning coils removed reduces the available phase angle operating space from 79% with no coils removed and a maximum current of 90 kAt to 27% with the maximum allowable current. Details of these results for the full set of coils, using either n=3 and n=4 perturbation fields, are discussed along with a summary of the effects of turning off a series of malfunctioning coils.

1. Introduction

Maintaining adequate control of the pedestal, scrape-off layer and divertor plasma properties in ITER is essential for safe and efficient operations as well as for meeting the scientific and technical objective of the project. One of the most demanding pedestal control issues in high confinement ITER H-mode plasmas is that of edge-localized modes (ELMs). ELMs are expected to produce repetitive energy pulses (ΔW_{ELM}) that are projected to release up to 20% of the stored pedestal plasma energy into the divertor plasma. In ITER, this implies that each ELM is capable of reaching a ΔW_{ELM} of up to 20 MJ during 15 MA Q_{DT}=10 H-mode plasmas with a total stored energy of 330 MJ. Based on the current understanding of materials limits exposed to these conditions, ΔW_{ELM} impulses of this magnitude will result in a significant reduction of the divertor target plate lifetime [1] and may produce impurities influxes leading to a substantial degradation of the core plasma performance or possibly to a disruptive termination of the discharge.

Starting with the first pedestal control experiments in DIII-D, using an external field-error correction coil (i.e., the C-coil) [2], it rapidly became evident that H-mode discharges are extraordinarily sensitive to small, $\delta B \sim 10^{-4}$-$10^{-3} B_T$, 3D magnetic field perturbations located near the surface of the plasma. Results from these initial experiments demonstrated that relatively small, mT level, intrinsic field-errors from the external confinement and shaping coils have the potential to significantly alter the performance tokamaks such as ITER. Subsequent DIII-D experiments with an in-vessel, non-axisymmetric, coil (i.e., the I-coil) proved that the stability of large Type-I ELMs could be modified by applying small 3D magnetic perturbation fields [3,4]. These results motivated the inclusion of a low toroidal mode number (n), in-vessel, non-axisymmetric control coil set in the ITER baseline design. The ITER coil, referred to as the ELM coil, is specifically designed to function as a versatile control tool for offsetting the effects of intrinsic 3D field-errors on the structure of the pedestal and for mitigating or suppressing large Type-I ELMs. As a consequence of its 3D field structure, the ITER ELM coil will modify the topology of the separatrix resulting in an effective mechanism for controlling the distribution of field lines intersecting the divertor target plates.

Although the ITER $n \leq 4$ ELM coil design, shown in Fig. 1, is primarily based on the DIII-D I-coil window-frame type coil geometry, it has several enhancements that provide additional operational flexibility. These include 9 coils in each toroidal row rather than the 6 coils per row used in DIII-D I-coil and a third row of window-frame type coils located on the equatorial plane. These extra coils make it possible to operate with n=4 perturbations and to smoothly rotate an n=3 sinusoidal field toroidally while holding the relative phase between each row of coils constant. This design also provide a sufficient level of redundancy needed in the event that random malfunctions occur in some of the individual window-frame coils making up the full 3×9 coil set geometry. The success of the DIII-D ELM suppression experiments along with the inclusion of the in-vessel ELM coil in the ITER baseline design has recently motivated a series of tokamak upgrades around the world in which various types low n in-vessel 3D window-frame type control coils have been installed. These include MAST with $n \leq 6$ coils [5], ASDEX-Upgrade with $n \leq 4$ coils [6] and KSTAR with $n \leq 2$ coils [7]. Experiments from these machines, along with recent DIII-D experiments, have significantly enhanced the international physics database of pedestal and ELM control results.

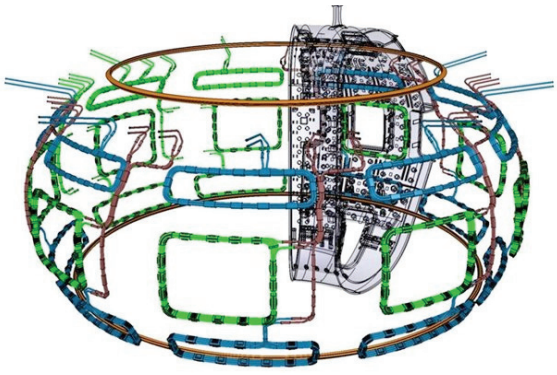

FIG. 1. The geometry of the internal (in-vessel) ITER ELM coil consisting of 3 toridal rows with 9 window-frame type coils in each row (i.e., a 3x9 coil). The centers of upper and lower rows of coils (shown in blue in the foreground and green in the background) are located at toroidal angles of ϕ_j=30°+40°j with j=0-8 in the ITER coordinate system, while the equatorial plane coils are located at ϕ_j= 26.7°+40°j with j=0-8. The upper and lower rows of coils have a relatively small aspect ratio, A = (poloidal height)/(toroidal length), compared to that of the equatorial row of coils.

As a prerequisite for the initial operation of the ITER ELM coil a detailed numerical study was undertaken to optimize the

operating parameters of the coil for various ITER discharge conditions using both n=4 and n=3 sinusoidal waveforms. An overview of the modeling objectives and approach used in this paper are discussed in Sec. 2 while Sec. 3 provides a summary of key results followed by a discussion of the conclusions drawn from these results.

2. ITER ELM Coil Modeling: Background and Methods

During the conceptual design phase of the ITER ELM coil various proposals were examined involving a variety of possible locations and coil geometries. These proposals were supported by numerical simulations of the magnetic field perturbations resulting from coils located outside the ITER vacuum vessel (ex-vessel coils) [8], between the double walls of the vacuum vessel (wall coils) [9], modular coils located inside port plugs (pp coils) [8,9], and various options for coils located behind the blanket modules inside the vacuum vessel (in-vessel coils) [8,9]. Based on these studies and physical constraints due to interfering obstacles located outside the vacuum vessel, coil maintainability requirements and the need to increase the coil current as the distance between the coils and the surface of the plasma increased, it was determined that the best option was to place the coils behind the blanket modules inside the vacuum as illustrated by the design shown in Fig.1.

Initial numerical studies of the vacuum magnetic perturbation field from the in-vessel ELM coil, shown in Fig. 1, were done using n=4 square and sinusoidal current waveform distributions described in Ref. [10]. These studies were carried out by superimposing the vacuum magnetic fields from the ELM coil on two CORSICA [11] equlibria: 1) a 15 MA H-mode, which is intended to be the standard operating scenario for the Q_{DT}=10 discharges in ITER, and 2) a 9 MA steady state discharge. Since these two equlibria have significantly different safety factor profiles $q(\psi_N)$, where ψ_N is the normalized poloidal magnetic flux function, they provided a good basis for an initial assessment of the flexibility of this particular coil design. Results from these initial studies verified that the 3×9 in-vessel ELM coil design is capable of matching the spectral properties of the DIII-D I-coil over a broad range of ITER discharge conditions [10].

2.1. Numerical Criteria Used to Evaluate the ITER ELM Coil Efficacy

A critical component required to evaluate of the efficacy of a particular non-axisymmetric coil design is a quantitative criterion based on a desired physics or engineering objective of the project. The primary technical objective of the ITER ELM coil design is to reduce the size of Type-I ELMs to a tolerable operating level as required by erosion limits specific to the materials used for the divertor target plates and main chamber plasma facing surfaces. This implies that the coil must mitigate Type-I ELMs or eliminate them completely by suppressing the onset of the ELM trigger mechanism. Since a fundamental physics understanding of ELM mitigation and suppression is not yet in hand, an empirical criterion based on data from DIII-D ELM-suppressed discharges was proposed [12] to quantify the Vacuum Island Overlap Width $\Delta_{VIOW}(\psi_N)$ across the edge of the plasma. This criterion is closely related to the Chirikov width parameter $\Delta_{Ch}(\psi_N)$ [2,10,13] and $\Delta_{Ch}(\psi_N)$ has been correlated with ELM suppression in DIII-D in a limited set of discharges [13]. Both the Δ_{VIOW} and the Δ_{Ch} parameters provide quantitative measures of the width of the vacuum stochastic field line

region from the separatrix inward toward the top of the pedestal. The Δ_{VIOW} parameter quantifies the width of the region covered by adjacent pairs of overlapping magnetic islands, without gaps between them, as shown in Fig. 2(a). Additionally, the Δ_{VIOW} parameter can be calculated automatically and is a more accurate measure of the width of the edge vacuum stochastic field region as the number of toroidal (n) and poloidal (m) modes included in the calculation is increased. Conceptually, the utility of these two parameters hinges on the premise that any coil set capable of producing an equivalent Δ_{VIOW} or Δ_{Ch} in plasmas similar to those used in DIII-D during ELM suppression [3,4,12-18], should produce a similar plasma response and thus lead to ELM suppression. In other words, if discharge conditions identical to those of a DIII-D discharge, that resulted in ELM suppression, are obtained in a machine with a coil capable of matching the DIII-D I-coil Δ_{VIOW} and Δ_{Ch} and possible as-yet unidentified parameters, it should be possible to obtain ELM suppression.

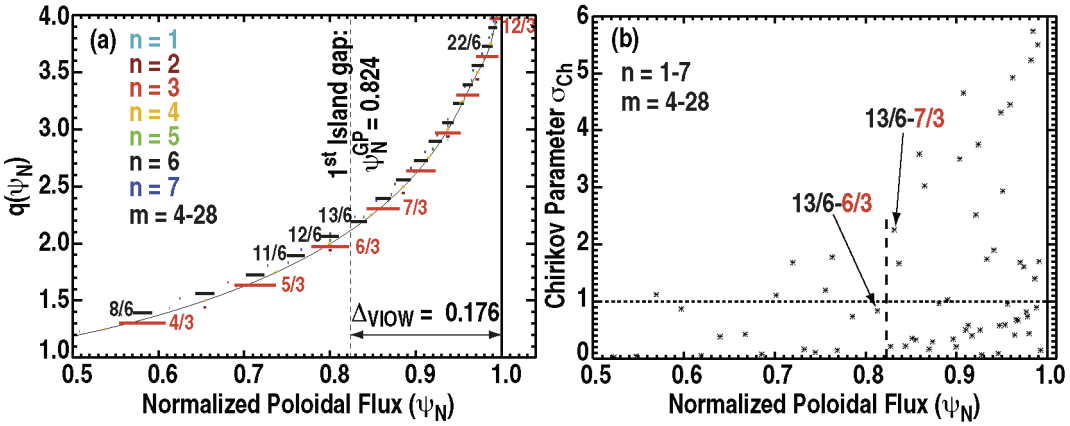

FIG. 2. (a) The locations and widths of various vacuum magnetic islands with polodal (m) and toroidal (n) mode numbers ranging between m=4 and 28, n=1 and 7 as a function of ψ_N. The width of the island overlap region Δ_{VIOW}, as determined by the 1st gap between adjacent islands, is indicated in the lower right-hand corner, (b) Chirikov parameter data for individual pairs of m,n islands shown in (a) using the same 15 MA ITER H-mode equilibrium with a peak current of 45 kAt in the ELM coil.

Figure 2(a) shows results from an automated calculation of Δ_{VIOW} using a 15 MA ITER equilibrium with a pedestal T_e=4.5 keV and a peak ELM coil current of 45 kAt in each row of the ITER ELM coil. This is the standard H-mode scenario that will be used for Q_{DT}=10 discharges where a pedestal T_e=4.5 keV is assumed to be the reference case for this scenario. Here, we see that the code found the first gap between adjacent pairs of neighboring islands, starting from the separatrix and moving inward toward the center of the plasma, located at $\psi_N^{GP} = 0.824$ resulting in $\Delta_{VIOW} = 1 - \psi_N^{GP} = 0.176$.

Figure 2(b) shows the equivalent Chirikov parameter distribution as a function of ψ_N. The Chirikov parameter is defined as $\sigma_{Ch} = (\Delta_{m,n}+\Delta_{m+1,n})/(\delta\psi_{N,m:m+1,n})$ where $\Delta_{m,n}$, $\Delta_{m+1,n}$ are the half-widths of adjacent m,n islands in ψ_N and $\delta\psi_{N,m:m+1,n}$ is the distance between these island pairs in ψ_N. A discussion of the method used to calculate $\Delta_{m,n}$ is given in Ref. 9. The Chirikov width parameter is defined as $\Delta_{Ch}(\psi_N) = 1 - \psi_N^*$ where ψ_N^* is determined by identifying the point where σ_{Ch}=1. As seen in Fig. 2(b), when the number of toroidal modes is increased in the calculation of σ_{Ch} small, high-m,n, neighboring islands do not overlap causing the value of σ_{Ch} for these pairs of islands to be less than 1. This creates an ambiguity when

attempting to interpret the data because larger, low-*m,n*, islands may still have $\sigma_{Ch}>1$ over this same region in ψ_N so an additional analysis of the data is needed to determine if gaps are present or, in other words, which pairs of islands are relevant for the determination of Δ_{Ch}. Since small high-*m,n* islands can fill gaps between large low-*m,n* islands in some situations, including more *m,n* modes in the calculation increases the accuracy of the width parameter. Another complication involved in using the Δ_{Ch} parameter is that multiple island resonances are sometimes located on the same rational surface. For example, the $m=2n$ islands for n=1-7 shown in Fig. 2(a) are all located at $\psi_N=0.8$ resulting in $\delta\psi_{N,m:m+1,n}=0$ for these pairs of islands and $\sigma_{Ch}=\infty$. Therefore, the analysis discussed in this paper is based on calculations of Δ_{VIOW} parameter as proposed in [12].

2.2. Description of Numerical Methods Used for Modeling the ITER ELM Coil

Since each of the window-frame coils that make up the ITER ELM coil has its own set of leads and a dedicated power supply, it is possible to configure the system with any arrangement of arbitrary currents in each window-frame coil. This has important advantages for the ITER project including to ability to isolate a malfunctioning window-frame coil from the rest of the system without requiring an opening of the vacuum vessel and the ability to individually specify currents in each of the 9 window-frame coils in a particular toroidal row to match a relatively pure sinusoidal waveform as discussed in Ref. [10]. For the purposes of the analysis done here, a 9-point discrete representation of either an n=3 or n=4 cosine waveform was used. The values chosen for the currents (I_j) in each of the j=0→8 window-frame coils, in a particular toroidal row, are calculated using the following equation:

$$I_j = I_o \cos\left[n\left(\phi_j - \Delta\phi\right)\right] \quad . \tag{1}$$

where I_o is the peak current in any coil having $\phi_j=\Delta\phi$, n is the desired toroidal mode number of the current distribution, ϕ_j is the location of the toroidal center angle of the j^{th} window-frame coil and the toroidal phase of the current is set using $\Delta\phi$. The centers of the upper and lower rows of window-frame coils are located at $\phi_j=30°+40°j$ with j=0-8 in the ITER coordinate system while the centers of the middle (equatorial plane) window-frame coils are located at $\phi_j=26.7°+40°j$ with j=0-8.

For the studies discussed here, the Δ_{VIOW} parameter is calculated when varying the toroidal phase of the currents in the upper and lower rows using 2° steps in $\Delta\phi$ while holding the current in the middle (equatorial plane) row constant. This allows us to find the minimum I_o required to satisfy the DIII-D ELM suppression correlation criterion and the extent of the available phase angle operating space for each current I_o given a particular operating scenario. For an n=3 waveform this results in a 60×60 array of Δ_{VIOW} parameter values between 0° and 118° or 3,600 data points for each I_o between 5 kAt and 90 kAt where 90 kAt is the maximum operating current of the ITER ELM coil. Thus, a total of 64,800 calculations similar to the one shown in Fig. 2(a) are required for each ITER operating scenario studied. Data from these calculations are displayed using a 2D color array, consisting of 2°×2° pixels, such as the one shown in Fig. 3(a). Using a ϕ=30° coordinate frame relative to that of the standard ITER system, we calculate the value of Δ_{VIOW} with window-frame coil currents

specified by Eq. (1) where the upper, lower and middle row phase angles are $\Delta\phi_{U,i}$=0º+2ºi for i=0-59, $\Delta\phi_{L,k}$=0º+2ºk for k=0-59 and $\Delta\phi_M$=0º.

The values of the Δ_{VIOW} parameter data shown in Fig. 3a were calculated using a CORSICA 15 MA ITER Q_{DT}=10 H-mode reference scenario equilibrium with a pedestal T_e=4.5 keV and a peak ELM coil current I_o=45 kAt in window-frame coils where ϕ_J=$\Delta\phi$. In this case, the maximum value of the Δ_{VIOW} parameter, Δ_{VIOW} = 0.176, is found with $\Delta\phi_U$=86º, $\Delta\phi_M$=0º and $\Delta\phi_L$=34º as shown by the intersection of dashed white lines in Fig. 3(a). This maximum in Δ_{VIOW} is typically found for several combination of $\Delta\phi$, which are indicated in plots such as Fig. 3(a) by the pixels located inside the solid white contour line. In addition, pixels with Δ_{VIOW} values grater than or equal to the DIII-D ELM suppression correlation criterion are located inside the solid black contour line shown in Fig. 3(a). Figure 3(b) shows the behavior of the maximum Δ_{VIOW} parameter as the peak ELM coil current is increased from 5 kAt to 90 kAt in 5 kAt steps. Each of the data points on this plot is determined using a plot similar to Fig. 3(a). In general, each step upward in the peak Δ_{VIOW} parameter results from closing a gap between two adjacent islands at a smaller ψ_N value. For example, the increase from Δ_{VIOW}= 0.176 at 45 kAt to Δ_{VIOW}=0.225 at 50 kAt with $\Delta\phi_U$=76º, $\Delta\phi_M$=0º and $\Delta\phi_L$=46º closes the gap between the m,n=13,6 and 6,3 islands at ψ_N=0.824 moving the position of the 1st gap inward to ψ_N=0.775 between the m,n=11,6 and 6,3 islands as seen in Fig. 2(a).

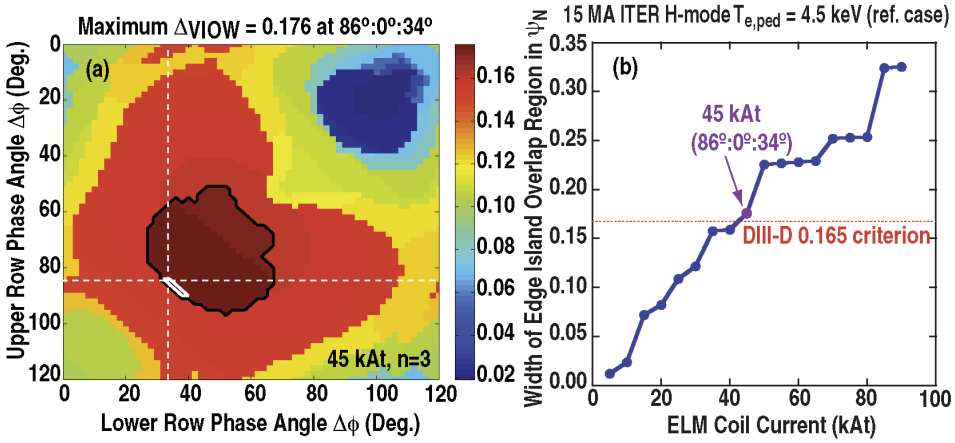

FIG. 3. (a) The Δ_{VIOW} parameter value, indicated by the color bar on the right, as a function of the toroidal phase $\Delta\phi$ in the upper coil row (y-axis) and the lower coil row (x-axis) with the middle coil row held constant. (b) Change in the Δ_{VIOW} parameter versus the peak ELM coil current.

3. Results and Conclusions

The n=3 analysis described above was carried out for each of the standard ITER operating scenarios shown in Table 1. Here, the minimum current I_o required to meet the DIII-D ELM suppression correlation criterion is shown in the 3rd column followed by the maximum Δ_{VIOW} at that current and a representative value of the upper, middle and lower phase angle settings ($\Delta\phi_U$:$\Delta\phi_M$:$\Delta\phi_L$) resulting in that Δ_{VIOW} is listed in the 5th column. The last column gives the percentage of pixels meeting or exceeding the DIII-D ELM suppression correlation criterion due to changes in toroidal phase of both the upper and lower row of coils as shown by the region inside the black contour in Fig. 3(a) compared the region outside the black contour. Case number 2 in the table corresponds to the results shown in Fig. 3 using the 15 MA

Q_{DT}=10 H-mode scenario with a pedestal T_e=4.5 keV. Cases 1-4 are similar except for the pedestal T_e. It is seen that the T_e = 3.5 keV case requires the largest I_o and that as T_e is increased up to 5.5 keV I_o is reduced. This results from an increase in the edge pressure gradient which drives more edge bootstrap current increasing the shear in the edge safety factor profile $q(\psi_N)$. At T_e=6.5 keV a flattening of $q(\psi_N)$ near ψ_N=0.96 causes I_o to increase.

Table 1
Summary of *n*=3 ELM Coil Results for Various ITER Operating Scenarios

No.	Scenario Name	I_0 (kAt)	Δ_{VIOW}	Optimal $\Delta\phi_U$:$\Delta\phi_M$:$\Delta\phi_L$ Phase Angle (Deg.)	Phase Angle Operating Space (%)
1	15 MA, 3.5 keV, Q_{DT}=10	50	0.2097	64:0:50	9.5404
2	15 MA, 4.5 keV, Q_{DT}=10	45	0.1757	86:0:34	7.579
3	15 MA, 5.5 keV, Q_{DT}=10	35	0.1702	70:0:50	2.0962
4	15 MA, 6.5 keV, Q_{DT}=10	40	0.1801	60:0:52	17.979
5	15 MA, 4.5 keV, Quasi-DN	45	0.1869	70:0:56	12.873
6	9 MA, SN, Q_{DT}=5	20	0.2069	34:0:84	22.951
7	10 MA, SN, rampdown	35	0.1730	54:0:60	5.8318
8	10 MA, SN, rampup	35	0.1831	44:0:76	0.2687
9	7.5 MA, SN, q_{95}=3.0	25	0.1837	88:0:28	16.877
10	9 MA, SN, Q_{DT}=5, β_p=1.25	25	0.1674	40:0:80	10.320

A similar analysis has been done for cases 1, 2, 3 and 5 in Table 1 using an *n*=4 cosine distribution in each of the three ELM coil rows. In this case, a trend similar to that of the *n*=3 results except I_o=75 kAt at T_e=3.5 keV then drops to 45 kAt and 35 kAt at T_e=4.5 keV and 5.5 keV respectively. In general, the *n*=4 waveform produces a more complex island structure compared to the *n*=3 waveform since it is not possible to simulate a pure *n*=4 waveform with 9 discrete window-frame coils. Thus, in an *n*=4 plot equivalent to Fig. 2(a) the small dots due to the higher *m,n* island are significantly larger resulting in a more asymmetric divertor footprint pattern and are somewhat more sensitivity to the opening of gaps as the toroidal phase angle of the coils is changed.

It may be necessary in some situations to turn off individual widow-frame coils if unanticipated malfunctions occur in those coils. Based on this prospect, a series of detailed analyses were carried out similar to those discussed above using the *n*=3 waveform with random window-frame coils turned off in various coil rows. Since the middle row (equatorial plane) window-frame coils drive more magnetic flux than the upper and lower coils, due to their larger area, these coils were turned off in a series of steps to determine how I_o scales with the number of coils being turned off. This was done using the most demanding scenario in Table 1 case 1 with T_e=3.5 keV. It was found that I_o increased from 50 kAt with no coils turned off to 55 kAt, 60 kAt and 70 kAt with 3, 4 and 5 of the middle row coils turned off respectively. Turning off 6 or 7 of the middle row coils increased I_o to 80 kAt. A small set of phase settings, with an operating space of 1.6%, was found with 8 middle row coils turned off and I_o=75 kAt while it was not possible to satisfy the DIII-D criterion with all 9 middle row coils turned off when using the maximum ELM coil I_o=90 kAt in the remaining two rows. Increasing I_o from 75 kAt to 90 kAt with 8 coils turned off in T_e=3.5 keV scenario opened up

the operating phase space from 1.6% to 27%, which still provides a reasonable degree of flexibility for configuring the remaining 19 window-frame coils but is a significant reduction from the available operating phase space of 79% with all 27 window-frame coils when using this ITER scenario. In general, it is found that in the vacuum field limit, the ITER ELM coil design is capable of producing 3D perturbations equivalent to those used in DIII-D for ELM suppression over a wide range of plasma parameters and $q(\psi_N)$ profiles with a sufficient coil current margin to accommodate malfunctions of up to 8 window-frame coils making up the full 3x9 ELM coil set.

In addition to these vacuum field results discussed above, a series of heat and particle transport studies have been carried out using a fluid plasma transport code coupled to a Monte-Carlo neutral transport code based on the n=3 analyses done in this paper [19]. Results from these simulations indicate a significant reduction of the peak ITER divertor heat flux during cases satisfying the DIII-D ELM suppression correlation criterion. Including the plasma response in the calculations discussed above is expected to lead to a reduction of the island widths (screening) or an increase in the island widths (amplification). These effects are being simulated using a nonlinear MHD code [19,20].

This work was supported by UT BATTELLE, LLC under 4000095588 and the US Department of Energy under DE-FG02-05ER54809, DE-FG02-07ER54917, DE-AC05-00OR22725 and ITER Task Agreement C19TD42FU.

The views and opinions expressed herein do not necessarily reflect those of the ITER Organization.

References

[1] LOARTE, A., et al., Plasma Phys. Control. Fusion **45** (2003) 1549.
[2] EVANS, T.E., et al., Phys. Plasmas **9** (2002) 4957.
[3] EVANS, T.E., et al., Phys. Rev. Lett. **92** (2004) 235003.
[4] EVANS, T.E., et al., Nucl. Fusion **45** (2005) 595.
[5] KIRK, A., et al., Nucl. Fusion **50** (2010) 034008.
[6] SUTTROP, W., et al., Phys. Rev. Lett. **106** 225004 (2011).
[7] JEON, Y. M., et al., Phys. Rev. Lett. **109** (2012) 035004.
[8] BECOULET, M., et al., Nucl. Fusion **48** (2008) 024003.
[9] SCHAFFER, M.J., et al., Nucl. Fusion **48** (2008) 024004.
[10] ORLOV, D.M., "Analysis Edge Magnetic field line Structure in ITER due to in-vessel ELM Control Coils," accepted for publication in Fusion Eng. and Design (2012).
[11] CROTINGER, J.A., et al., "Corsica; A Comprehensive Simulation of Toroidal Magnetic-fusion Devices," Lawrence Livermore National Laboratory Technical Report UCRL-ID-126284 (1997).
[12] EVANS, T.E., Nucl. Fusion **48** (2008) 024002.
[13] FEMSTERMACHER, M.E., Phys. Plasmas **15** (2008) 056122.
[14] EVANS, T.E., et al., Nature Phys. **2** (2006) 419
[15] MOYER, R.A., Phys. Plasmas **12** (2005) 056119.
[16] BURRELL, K.H., Plasma Phys. Control. Fusion **47** (2005) B37.
[17] SCHMITZ, O., et al., Phys. Rev. Lett. **103** (2009) 165005-1.
[18] EVANS, T.E., et al., Phys. Plasmas **13** (2006) 056121.
[19] SCHMITZ, O., et al., "Three-dimensional Fluid Modeling of Plasma Edge Transport and Divertor Heat and Particle Loads During RMP ELM Control at ITER", this conference, paper ITR/P1-24.
[20] LOARTE, A., et al., "Progress on the Application of ELM Control Schemes to ITER," this conference, paper ITR/1-2.